water

MDPI

Article

Effect of Flow Interference between Cylinders Subjected to a Cross Flow over a Cluster of Three Equally Spaced Cylinders

Jia Dong [1,*], Xianrui Shi [2] and Genhua Yan [1]

[1] Nanjing Hydraulic Research Institute, Nanjing 210029, China; ghyan@nhri.cn
[2] Development Research Center of the Ministry of Water Resources of P. R. China, Beijing 100038, China; shixianrui56@gmail.com
* Correspondence: jdong@nhri.cn

Abstract: In this paper, flow over a cluster of three equally spaced circular cylinders was studied by numerical simulation based on the turbulence model k-kl-ω for two incidence angles β = 0° and 60°, at different Reynolds numbers, and flow interference pattern characteristics between cylinders, characteristics of force parameters, and Strouhal number of each cylinder with different spacing ratios ranging from 1.5 to 4 at Re 8×10^4, 2×10^5 and 2×10^6 were obtained. Analyzing the flow field around three cylinders, the following results have been obtained: (1) at incidence angle β = 0° and 60°, the wake was nearly symmetrical if S/D ≥ 2.0; (2) at β = 60°, S/D = 1.5, and Re = 2×10^5, an asymmetric periodic flow pattern occurred in the wake region which produced a significant effect on the surface mechanical parameters and Strouhal number, and this was observed for the first time. The periodic flow regime of the wake region also occurred at S/D = 1.35 and 1.5, without the same phenomenon at S/D = 1.7 and 2.0; this phenomenon is described for the first time in this paper; (3) the phenomenon of periodic flow regime in the wake region was intrinsic and related to Reynolds number and space ratio. In addition, the characteristics of force parameters of three cylinders were mainly affected by the interference between cylinders, at 1.5 < S/D < 4, which indicated that the drag coefficient of three cylinders reduces with different Reynolds numbers and increases with enlargement of the spacing ratio for upstream cylinders at incidence angle 0°. At incidence angle 60° and S/D = 1.5~4, the Strouhal number decreases with the enlargement of spacing ratio for the upstream cylinders, but the Strouhal number increases for the downstream cylinder, which is another prominent flow interference influence. The results indicated the effect of flow interference between cylinders subjected to a cross flow over a cluster of three equally spaced cylinders, considering the flow pattern, surface mechanical parameters and Strouhal number, which should be considered in the establishment of standard design codes in fields such as offshore wind turbine engineering for flow interference around groups of cylinders.

Keywords: three equally spaced cylinders; flow interference; spacing ratio; incidence angle; periodic flow regime

check for updates

Citation: Dong, J.; Shi, X.; Yan, G. Effect of Flow Interference between Cylinders Subjected to a Cross Flow over a Cluster of Three Equally Spaced Cylinders. *Water* **2024**, *16*, 2165. https://doi.org/10.3390/w16152165

Academic Editor: Giuseppe Pezzinga

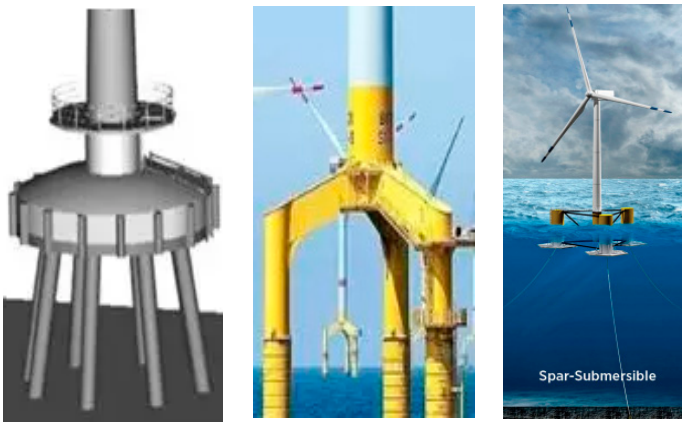
Received: 13 June 2024
Revised: 25 July 2024
Accepted: 29 July 2024
Published: 31 July 2024

Copyright: © 2024 by the authors. Licensee MDPI, Basel, Switzerland. This article is an open access article distributed under the terms and conditions of the Creative Commons Attribution (CC BY) license (https://creativecommons.org/licenses/by/4.0/).

1. Introduction

Interaction between fluid flow and cylindrical bodies is seen in multiple engineering applications. Therefore, there are numerous investigations of flow over uniform single circular cylinders [1–9]. Many of the previous studies focused on the vortex shedding phenomenon, which results in periodic loading. However, modern engineering applications usually involve fluid flow interaction with multiple cylinders, such as ocean engineering, pile design of offshore wind turbines, and so on. In practical applications, pile foundations of offshore wind turbines are mostly used. Pile foundations include single pile, three piles, and four piles, as well as grouped rings of piles in a bearing platform structure and multi-pile floating foundations. Under the action of tidal current, interference flow patterns occur in the flow around the pile groups, which affects the characteristics of surface mechanical

parameters. A typical three-piles foundation is shown in Figure 1. The interference flow pattern, effect of spacing ratio, incidence angle, and different Reynolds numbers have been researched in papers [10–17] which indicate the variation rules of drag and lift coefficient, the Strouhal number and the surface pressure coefficient with spacing ratio and incidence angle of different three-cylinder arrangements in subcritical regimes. The flow interference characteristics were studied by A. T. Sayers [10] at Re = 3×10^4, S/D = 1.25~5, and different incidence angles. Zdravkovich [11] indicated that the total force coefficients for three cylinders as a unit show large variation in direction and spacing ratios, and this paper also indicates this point by analyzing the pressure coefficient distributions around cylinders. At Re = 2.1 and 3.5×10^3 and S/D = 1.27~5.43, K. Lam and W. C. Chung studied the flow over a cluster of three equally spaced cylinders [16]. At $\beta = 0°$ and S/D = 1.27~2.29, there is a bi-stable wake behind the two downstream cylinders [14,16], but at Re = 3×10^4 and 5.1×10^4, this phenomenon does not occur [10], and in the current study at Re = 8×10^4. In addition, the drag coefficient and Strouhal number of the flow around three cylinders are also different from the values observed in a single cylinder. At incidence angle $\beta = 0°$, the value of the drag coefficient C_D increases with the enlargement of the spacing ratio for the upstream cylinder and increases for the two downstream cylinders [12,13,17] if Re = 100, 200 and 6.08×10^4, and the same result is given in this paper when the Reynolds number is 8×10^4 and S/D = 1.5~4. Nevertheless, the Strouhal number reduces with increasing spacing ratio at Re = 2.1 and 3.5×10^3 for the upstream cylinders, and the opposite for downstream cylinders [16]; the same results are given in this paper with different Reynolds numbers, but the Strouhal number increases with the enlargement of spacing ratio at Re = 100, 200 [13,15].



(**a**) (**b**) (**c**)

Figure 1. Fixed- and float-pile foundations of offshore wind turbines: (**a**) multiple pile cap foundation; (**b**) three pile foundation; (**c**) float-three-pile foundation.

The present investigation focuses on cross-flow over a cluster of three equally spaced cylinders. The flow development results in complex vortex interactions and multiple frequency-centered activities in the wake region. Previous investigations have shown that the pattern of the wake region and characteristics of surface mechanical parameters are governed primarily by the spacing ratio between the cylinders (S/D), incidence angle, and Reynolds numbers. However, the study above focuses on the subcritical regime; for critical and supercritical regimes, research results are rare. In this paper, the different Reynolds numbers for different regimes (Re = 3×10^4, 8×10^4, 2×10^5, 5×10^5, 2×10^6, 4×10^6) are studied with different spacing ratios (S/D = 1.5~4) at different incidence angles ($\beta = 0°$, 20°, 40°, 60°), the pattern of the wake region and characteristics of surface mechanical parameters are analyzed to indicate the intrinsic laws due to the interference effect among cylinders by the numerical simulation method, and the variation laws for drag and lift coefficient, pressure coefficient distribution, and Strouhal number are obtained.

2. Numerical Simulation Method and Validity Checking

The study is performed using the numerical simulation method, and this section verifies the turbulence model and validity of the simulation method.

2.1. Governing Equation

For a viscous incompressible fluid, the governing equations include the continuity equation and momentum equation [13], which are written as follows:

Continuity equation:

$$\rho \frac{\partial u_{\mathrm{i}}}{\partial x_i} = 0 \tag{1}$$

Momentum equation:

$$\rho \frac{\partial u_{\mathrm{i}}}{\partial t} + \rho u_j \frac{\partial u_{\mathrm{i}}}{\partial x_{\mathrm{j}}} = -\frac{\partial p}{\partial x_{\mathrm{i}}} + \frac{\partial}{\partial x_{\mathrm{j}}}\left(\mu \frac{\partial u_{\mathrm{i}}}{\partial x_{\mathrm{j}}}\right) \tag{2}$$

In the equations, ρ, u_i, p, μ, S_i represent the velocity component, the fluid density, time, pressure, fluid dynamic viscosity, and source item, respectively.

2.2. Turbulence Model and Its Selection for Numerical Simulation

2.2.1. Three Turbulence Models Selected

For simulating the flow around the cylinder, three turbulence models are selected: two-equation models, Realizablek-ε and SSTk-ω, and the k-kl-ω three-equation model.

(1) Realizablek-ε two-equation model:

$$\frac{\partial(\rho k)}{\partial t} + \frac{\partial(\rho u_j k)}{\partial x_j} = \frac{\partial}{\partial x_j}\left(\left(\mu + \frac{\mu_t}{\sigma_k}\right)\frac{\partial k}{\partial x_j}\right) + G_k + G_b - \rho\varepsilon - Y_M + S_k \tag{3}$$

$$\frac{\partial(\rho\varepsilon)}{\partial t} + \frac{\partial(\rho u_j \varepsilon)}{\partial x_j} = \frac{\partial}{\partial x_j}\left(\left(\mu + \frac{\mu_t}{\sigma_k}\right)\frac{\partial \varepsilon}{\partial x_j}\right) + \rho C_1 S\varepsilon - \rho C_2 \frac{\varepsilon^2}{k + \sqrt{v\varepsilon}} + C_{1\varepsilon}\frac{\varepsilon}{k} C_{3\varepsilon} G_b + S_\varepsilon \tag{4}$$

$$C_1 = \max\left[0.43, \frac{\eta}{\eta + 5}\right], \eta = S\frac{k}{\varepsilon}, S = \sqrt{2S_{ij}S_{ij}}, \mu_t = \rho C_\mu \frac{k^2}{\varepsilon} \tag{5}$$

$$C_\mu = \frac{1}{A_0 + A_S \frac{kU^*}{\varepsilon}}, U^* = \sqrt{S_{ij}S_{ij} + \widetilde{\Omega}_{ij}\widetilde{\Omega}_{ij}}, A_0 = 4.04, A_S = \sqrt{6}\cos\varphi \tag{6}$$

In Equations (5) and (6), C_μ is a variable quantity rather than constant, which is decided by the shear tensor, rotation tensor, kinetic energy and dissipation rating rather than constant 0.09, so that the equation can simulate large deformation flow.

(2) Two-equation model SSTk-ω considering shear rating [18]:

$$\frac{\partial}{\partial t}(\rho k) + \frac{\partial}{\partial x_i}(\rho k u_i) = \frac{\partial}{\partial x_j}\left[\left(\mu + \frac{\mu_t}{\sigma_k}\right)\frac{\partial k}{\partial x_j}\right] + G_k - \beta^*\rho\omega k + S_k \tag{7}$$

$$\frac{\partial}{\partial t}(\rho\omega) + \frac{\partial}{\partial x_i}(\rho\omega u_i) = \frac{\partial}{\partial x_j}\left[\left(\mu + \frac{\mu_t}{\sigma_\omega}\right)\frac{\partial \omega}{\partial x_j}\right] + 2\rho(1 - F_1)\frac{1}{\sigma_{\omega 2}\omega}\frac{\partial k}{\partial x_j}\frac{\partial \omega}{\partial x_j} - \beta\rho\omega^2 + S_\omega + G_\omega \tag{8}$$

$$\mu_t = a^*\frac{\rho k}{\omega}\frac{1}{\max\left[\frac{1}{a^*}, \frac{SF_2}{a_1\omega}\right]}, a^* = a^*_\infty\left(\frac{a^*_0 + Re_t/R_k}{1 + Re_t/R_k}\right), F_2 = \tanh\left(\phi_2^2\right), \phi_2 = \max\left[2\frac{\sqrt{k}}{0.09\omega y}, \frac{500}{\rho y^2\omega}\right] \tag{9}$$

In the two-equation model SST k-ω, the shear rating $SF_2/(a_1\omega)$ is factored into the turbulence viscosity μ_t, which accurately simulates the boundary layer separation flowing across a smooth wall.

(3) Three-equation model k-kl-ω [19]:

Based on the two-equation model, the equation for describing the laminar flow kinetic energy k_L is factored into the equations depicting turbulence flow, considering the transition of the boundary layer leading to the variation of the laminar flow kinetic energy:

$$\frac{Dk_T}{Dt} = P_{K_T} + R + R_{NAT} - \omega k_T - D_T + \frac{\partial}{\partial x_j}\left[\left(v + \frac{a_T}{a_k}\right)\frac{\partial k_T}{\partial x_j}\right] \tag{10}$$

$$\frac{Dk_L}{Dt} = P_{K_L} - R - R_{NAT} - D_L + \frac{\partial}{\partial x_j}\left[v\frac{\partial k_L}{\partial x_j}\right] \tag{11}$$

$$\frac{D\omega}{Dt} = C_{\omega 1}\frac{\omega}{k_T}P_{K_T} + \left(\frac{C_{\omega R}}{f_W} - 1\right)\frac{\omega}{k_T}(R + R_{NAT}) - C_{\omega 2}\omega^2 + C_{\omega 3}f_\omega a_T f_W^2\frac{\sqrt{k_T}}{d^3} + \frac{\partial}{\partial x_j}\left[\left(v + \frac{a_T}{a_\omega}\right)\frac{\partial \omega}{\partial x_j}\right] \tag{12}$$

2.2.2. Comparison between Simulation Results of Different Turbulence Models

(1) Mesh Generation and Time Step

Farrant et al. [6] indicated that a computational domain with 16D upstream, 14D downstream and 10D on either side of the cylinders could provide a better compromise between accuracy and computational costs for the flow around the cylinders. With the development of computer techniques, larger computational domains and greater mesh quantities are adopted to simulate the flow around the cylinder more accurately. The computational domain and grid model are shown in Figure 2, the width being 31 times and length being 46 times the diameter of the cylinder. The inlet is defined as the velocity inlet boundary; the outlet is a specified constant pressure; the left and right of the area and the surface of the cylinder are the specified no-slip wall boundary. To determine the pressure, shear stress, and separation degree of the surface of the cylinder for different turbulence models, a boundary layer grid is adopted near the cylinder surface (the first layer height being 10^{-5} m, $Y^+ = 0.22$), and the dimensionless time step has the value 0.01 ($V\Delta t/D = 0.01$) [13].

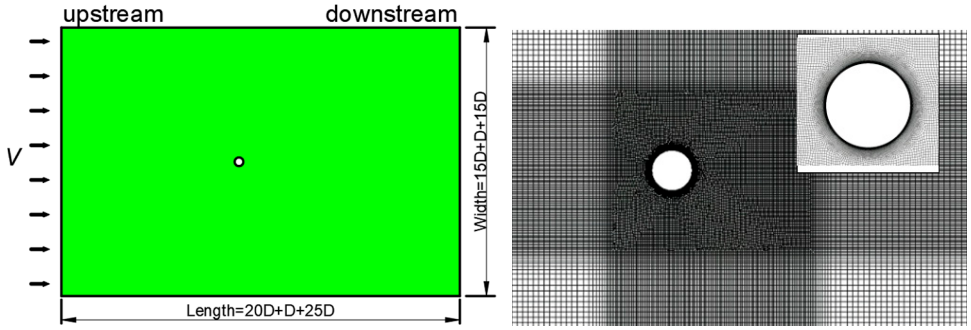


Figure 2. Computational domain model and grid model.

(2) Comparison of simulation results among different turbulence models

During the calculation, $Re = 4 \times 10^4$ is adopted to simulate the flow around the cylinder for comparing the roughness efficient C_D, Strouhal number St, pressure efficient C_p, and boundary separation angle θ_s; the comparison results are shown in Table 1. N. Mulvany et al. [20], Filipe S. Pereira et al. [9] and F. R. Meter [21] analyzed the effect on the numerical results of different turbulence models. N. Mulvany indicated that the

Realizablek-ε model could simulate the wing boundary layer problem more accurately than the SSTk-ω model for high Re number, and F. R. Meter indicated that the SSTk-ω model leads to a larger surface shear stress. In Table 1, the model drag coefficient for the Realizablek-ε model is smaller (62%), the root-mean-square value of the lift coefficient pulsation is smaller (107%), the Strouhal number St is larger (45.5%), the angle of separation is larger (25%), and the basal pressure coefficient C_{pb} is smaller than the test value (47.5%); the drag coefficient for SSTk-ω model is larger (3%), the root-mean-square value of the lift coefficient pulsation is larger (70%), the Strouhal number St is larger (26.5%), basal pressure coefficient C_{pb} is larger (25.4%), and the separation angle is moderate; the drag coefficient for the k-kl-ω model is close to the value of 1.18 [1] (5%), there is less error for the root-mean-square value of the lift coefficient pulsation (0.3% [5]), the Strouhal number St is a little smaller than Unal U.'s result of 0.186 (7.5% [7]), the basal pressure coefficient C_{pb} is similar to the results of N. Mulvany and Anatol Roshko at −1.18 (5% [2,20]), and the separation angle is close to E. Achenbach et al.'s result [3] (0.6%). The comparison results in Table 1 show the k-kl-ω model simulates better results for flow around the cylinder, therefore the model is adopted to analyze the flow around three equally spaced cylinders in a critical regime.

Table 1. Comparison and verification data of turbulence models.

Researcher	Re/10^4	C_D	C'_L	St	C_{pb}	C_{pmin}	θ_s
Ivette Rodriguez [6]/LES	4.2	0.994	0.316	0.214	−1.024	−1.548	87.5
N. Mulvany [20]/test	4.2				−1.18	−1.241	
U. Unal [7]	4.1	1.14		0.186			
E. Achenbach [3]	6	1.23					81.5
C. Wieselsberger [1]	3~4.2	1.18					
Anatol Roshko [2]	10				−1.18		
C. Norberg [4]	4		0.495	0.189			
Gonter Schewe [5]	4	1.1	0.352	0.2			
Alessandro Capone [8]	6.9						95~104
Current work							
Realizablek-ε model	4	0.722	0.17	0.275	−0.8	−1.85	102~105
SSTk-ω model	4	1.21	0.598	0.239	−1.48	−1.92	80~95
k-kl-ω model	4	1.12	0.353	0.172	−1.12	−1.394	82

2.3. The Grid and Its Validity Checking

Considering the bunching effect of the pile cluster, a larger computation domain is selected to avoid blockage effects on flow. Figure 3 shows the computation domain and grid of three piles, and Figure 4 shows the arrangement for three cylinders. The spacing between upstream of cylinder and inlet boundary is 20D; the spacing between downstream of cylinder and outlet boundary is 30D; the spacing between side wall and surface of cylinder is 10D. The inlet is defined as the velocity inlet boundary; the outlet is a specified constant pressure; the left and right of the area and the surface of the cylinder are specified as a no-slip wall boundary. To determine the pressure, shear stress and separation degree of the cylinder surface for different turbulence models, a boundary layer grid is adopted near the cylinder surface (the first layer height being 10^{-5} m, $Y^+ = 0.22$), and the dimensionless time step has the value 0.01 ($V\Delta t/D = 0.01$) [13].

Considering the effect of the number of cells, three different-sized grids are designed to analyze the impact on the mean roughness efficient C_D. In Table 2, the number of cells reaches 430,000, and the variation of C_D satisfies the accuracy of the simulation, error being 1%.

The verification of the simulation results is shown in Table 3. Analyzing the data of Table 3, at Re = 8×10^4, the C_D result of the current work approaches that of the study by S. G. Pouryoussefi et al. [12], error being 3%; at Re = 3×10^4, the C_D and St results of the current work approach the data of A. T. Sayers [10], error being 2% and 4%, respectively.

From Table 3, it can be seen that the results of this paper are basically consistent with previous results, which proves that the numerical method and parameter settings of this paper are reasonable and feasible.

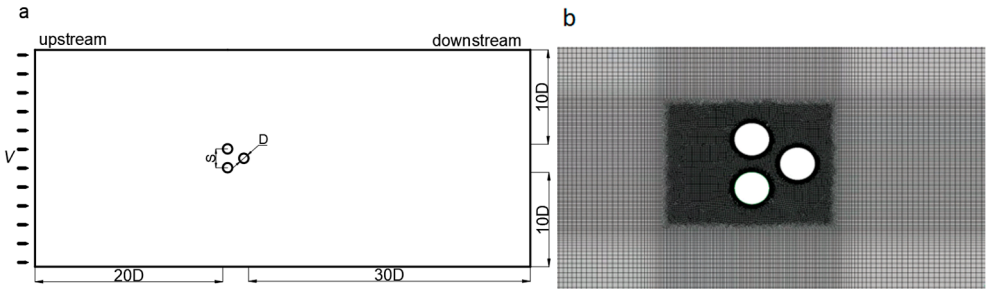


Figure 3. Computation domain and grid of three piles: (**a**) diagram of computation domain for three equally spaced cylinders; (**b**) grid of three cylinders β = 60°.

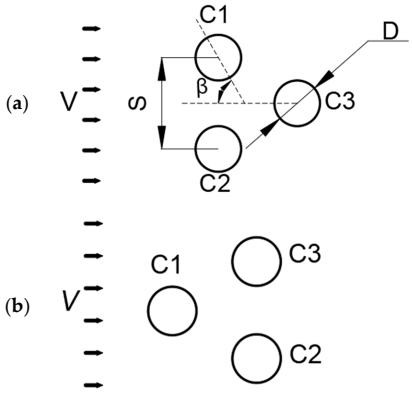


Figure 4. Arrangement for three cylinders: (**a**) position of cylinders, β = 60°; (**b**) position of cylinders, β = 0°.

Table 2. Calculation results of different grid scales.

Mesh	Re/10^4	S/D	Incidence Angle/°	Number of Cells	C_D (C1, C2, C3)
Mesh 1	8.0	1.5	0	80,000	0.68/0.747/0.749
Mesh 2	8.0	1.5	0	210,000	0.727/0.812/0.811
Mesh 3	8.0	1.5	0	430,000	0.735/0.811/0.807

Table 3. Validation results.

Researcher	Re/10^4	S/D	Incidence Angle/°	C_D (C1, C2, C3)	St_A	St_B	St_C
S. G. Pouryoussefi et al. [12]	6.08	2.5	0	0.82/1.08/1.05	0.336	0.181	0.181
A.T.Sayers [10]	3.0	1.5	0	0.75/0.769	0.274	0.175	0.175
Current work	3.0	1.5	0	0.735/0.811/0.807	0.263	0.183	0.183
Current work	6.08	2.5	0	0.846/0.982/0.98			

3. Simulation Results

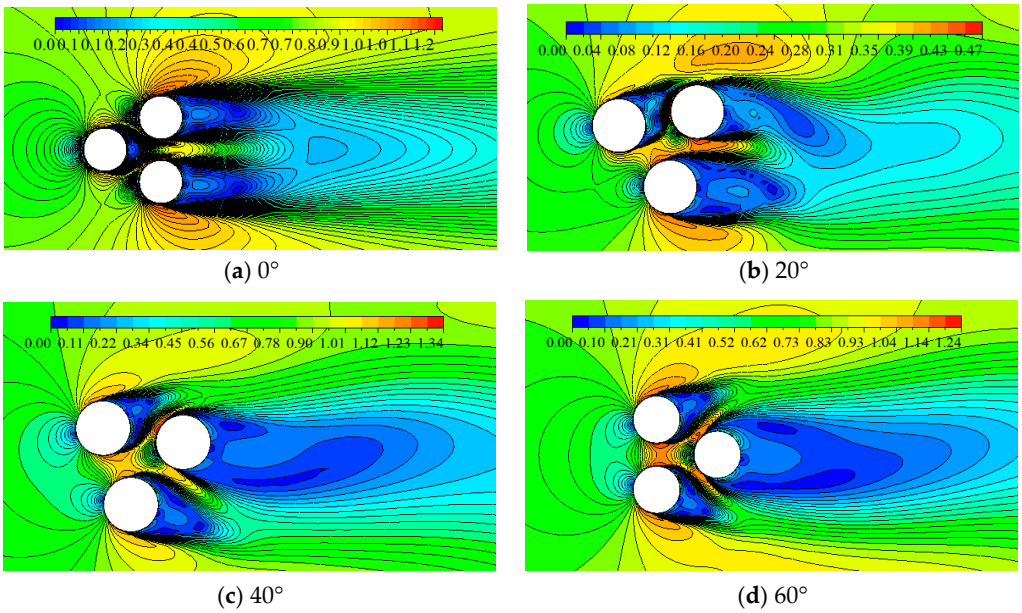
3.1. Flow Interference Pattern Characteristics among Cylinders

3.1.1. Effect of Spacing Ratio S/D on the Flow Pattern

The effect of interference is the fundamental characteristic distinguishing the flow through a cluster of three equally spaced cylinders from the flow past a circular cylinder, which changes with the variations of spacing ratios, incidence angles to the free stream, and Reynolds number. Zdravkovich [11] (60 < Re < 300) indicates that when the Re is

a constant, the flow interference pattern among piles is divided into three categories: (1) Proximity interference, which takes place when the distance between the cylinders is small enough. (2) Wake interference, which generates around downstream cylinders completely or partially submerged in the wake of others. (3) Combined interference, which represents wake and proximity interference [13]. The present investigation also reveals similar interference characteristics with the variation of spacing ratio at Re = 8×10^4.

Figure 5 shows the instantaneous velocity contours for flow field at S/D = 1.5 and Re = 8×10^4, with four different incidence angles (β = 0°, 20°, 40°, 60°). The wake of the upstream cylinder is suppressed by the cylinder downstream and proximity interference dominates the flow. In addition, the incidence angle also significantly affects the flow pattern: (1) a symmetrical form appears in wake of the cylinders downstream at β = 0°, 60° (Figure 5a,d); (2) an asymmetrical form appears in the wake of the cylinders downstream at β = 20°, 40° (Figure 5b,c); (3) a bi-stable regime is not observed at β = 0° (Figure 3a), which illustrates that Reynolds number can have a significant effect on the onset of the bi-stable flow regime, and the numerical research by Bao et al. [15] showed no bi-stable flow at Re = 100 for approximately the same spacing ratios as those studied by Lam and Cheung [16].



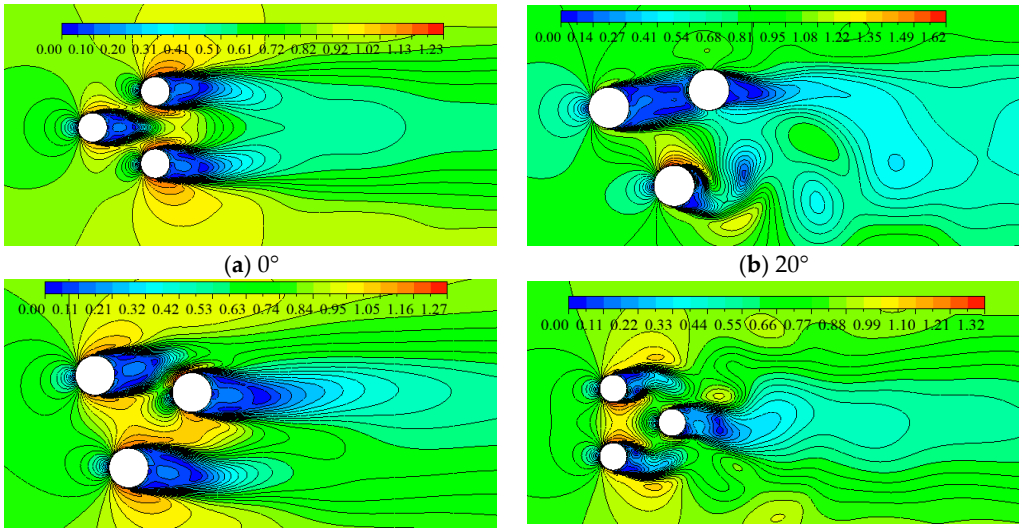
(**a**) 0° (**b**) 20°

(**c**) 40° (**d**) 60°

Figure 5. Contours of velocity with different incidence angles: S/D = 1.5, Re = 8×10^4.

At S/D = 2.5, which is selected as an intermediate spacing ratio, the flow interference is dominated by the suppression between cylinders and interference of the wake. Figure 6 shows the instantaneous velocity contours for flow field at S/D = 2.5 and Re = 8×10^4, with four different incidence angles (β = 0°, 20°, 40°, 60°). The suppression and the gap stream between cylinders dominates the flow field at β = 0°, 40°, just as Figure 6a,c display, but the interference of the wake is significantly affected by the flow pattern at β = 20°, 60°, just as Figure 6b,d display.

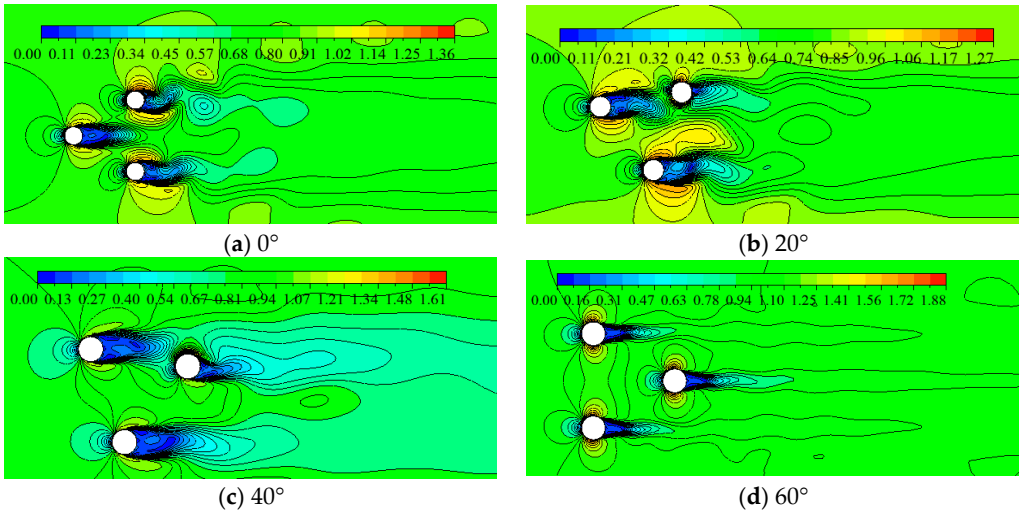
Enlarging the spacing ratio S/D, at S/D = 4, the interference of wake between cylinders controls the flow pattern, just as Figure 7 shows. Figure 7 shows the instantaneous velocity contours for flow field at S/D = 4 and Re = 8×10^4, with four different incidence angles (β = 0°, 20°, 40°, 60°). At β = 0°, a shedding vortex appears in the wake flow over three cylinders because of the wake of the downstream cylinders; the wake of the C1 cylinder is affected by cylinder C3 primarily at β = 20°; the effect of suppression between cylinders is very weak for the flow field, and the interference of wake plays an important role at β = 40°, 60°.



(**a**) 0° (**b**) 20°

(**c**) 40° (**d**) 60°

Figure 6. Contours of velocity with different incidence angles: S/D = 2.5, Re = 8×10^4.



(**a**) 0° (**b**) 20°

(**c**) 40° (**d**) 60°

Figure 7. Contours of velocity with different incidence angles: S/D = 4, Re = 8×10^4.

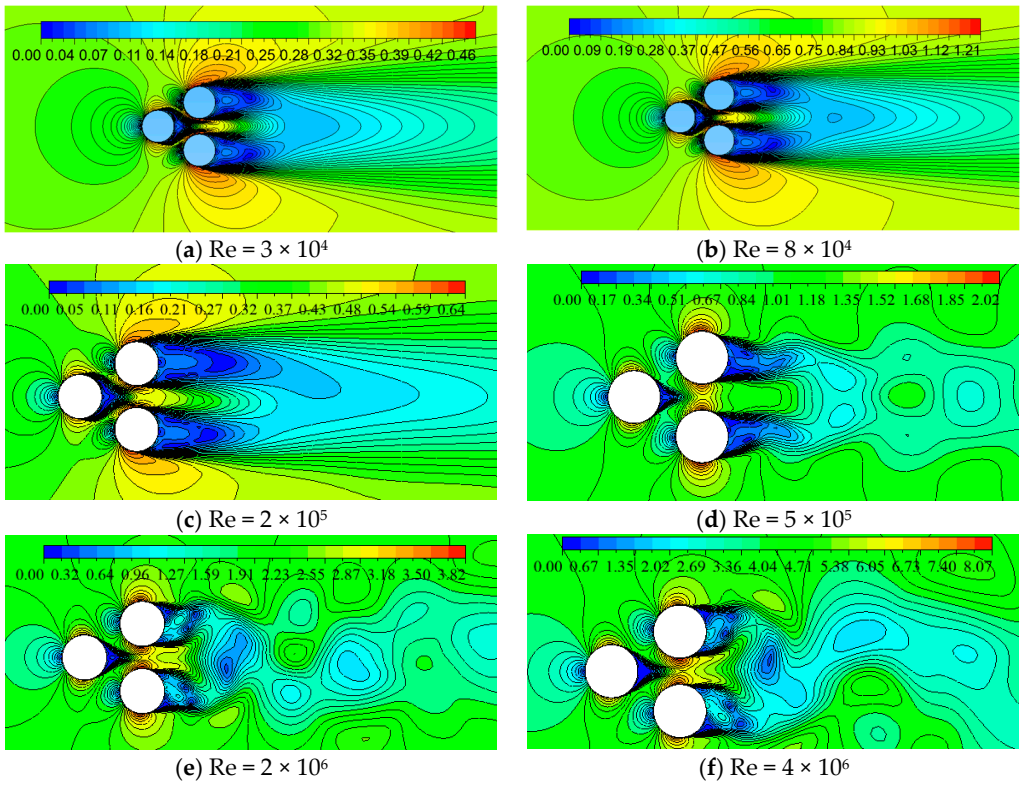
The spacing ratio and incidence angle are both very important parameters affecting the flow pattern over three cylinders, but the Reynolds number is another factor significantly impacting the flow regime, just as M. S. Bansal et al. [14] indicate.

3.1.2. Effect of Reynolds Number

It is well known that the flow regime and force characteristics change with the Reynolds number for flow past a single cylinder, which is divided into subcritical regime, critical regime, supercritical regime, and postcritical regime in terms of turbulence regimes [17]. Similarly, flow through a cluster of three equally spaced cylinders is also transformed under different Reynolds numbers.

Figure 8 shows the instantaneous velocity contours for flow field at S/D = 1.5 and $\beta = 0°$, with six different Reynolds numbers (Re = 3×10^4, 8×10^4, 2×10^5, 5×10^5, 2×10^6, 4×10^6, corresponding to subcritical regime, critical regime, supercritical regime, and postcritical regime, respectively). At Re = 3×10^4, 8×10^4, 2×10^5, the wake of the cylinders downstream (C2 and C3) exhibits symmetrical features, and a bi-stable flow regime did not appear in the present investigation. At Re = 5×10^5, 2×10^6, 4×10^6 (supercritical and postcritical regimes), the combined shedding vortex between two cylinders downstream appears in the wake of flow past three cylinders, but the frequency and spacing distance

between vortex centers vary with Reynolds number, just as Figure 8d–f shows. Another obvious feature is that at Re = 5×10^5, 2×10^6, the vortex street is nearly symmetrically distributed in a transversal direction and shows asymmetrical distribution at Re = 4×10^6.



(**a**) Re = 3×10^4 (**b**) Re = 8×10^4

(**c**) Re = 2×10^5 (**d**) Re = 5×10^5

(**e**) Re = 2×10^6 (**f**) Re = 4×10^6

Figure 8. Contour of velocities with Re (S/D = 1.5, β = 0°).

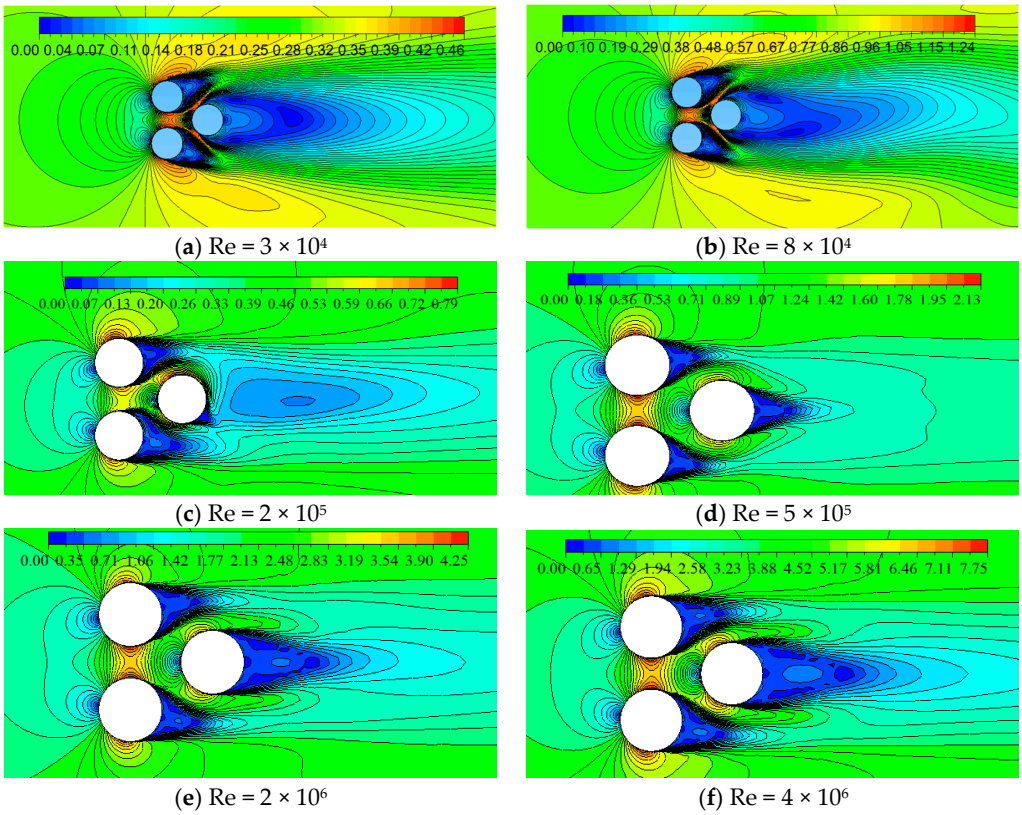
At S/D = 1.5 and β = 60°, with different Reynolds numbers (Re = 3×10^4, 8×10^4, 2×10^5, 5×10^5, 2×10^6, 4×10^6), the instantaneous velocity contours for flow field are shown in Figure 9. The figure indicates that at Re = 3×10^4, 8×10^4, 5×10^5, 2×10^6, 4×10^6, the flow fields exhibit near-perfect symmetry when the cylinder downstream (C3) suppresses the wakes of the cylinders (C1 and C2) upstream. But at Re = 2×10^5, the wake of the cylinder downstream (C3) displays asymmetrical features, and a typical vortex appears downstream from cylinder C3, just as Figure 9c shows. For the flow regime at Re = 2×10^5, β = 60° and different spacing ratios, the paper follows up with further study of its characteristics and force parameters by 2D and 3D numerical simulation; the study indicates that the flow regime exhibits periodic feathering, namely, the same wake of flow over three cylinders occurs periodically (if the period is T), which is elaborated in Section 3.1.3.

3.1.3. Characteristics of Periodic Flow Regime of the Wake Region Past Three Cylinders—Verification of Three-Dimensional Flow Field

At Re = 2×10^5, β = 0°, the flow pattern of the wake region is similar to that of the subcritical region at Re = 8×10^4. At S/D = 1.5 and β = 0°, there is no bi-stable flow regime in the wake region; but at β= 60°, the periodic flow regime of the wake region past three cylinders is first observed, having not yet been introduced nor explained in the existing literature. In this paper, it is believed that this periodic flow regime of the wake region past three cylinders is caused by the coupling of Reynolds number-reduced wake and limited spacing ratio.

Considering the study above at Re = 2×10^5, β = 60°, S/D = 1.5 being verified by the two-dimensional flow field, to verify the authenticity of the results, the study has also

been performed using three-dimensional flow field. In addition, whether the periodic flow regime of the wake region occurs only in a particular spacing ratio range is also analyzed.



(**a**) Re = 3 × 10^4 (**b**) Re = 8 × 10^4

(**c**) Re = 2 × 10^5 (**d**) Re = 5 × 10^5

(**e**) Re = 2 × 10^6 (**f**) Re = 4 × 10^6

Figure 9. Contours of velocities with Re (S/D = 1.5, β = 60°).

Figure 10 shows the arrangement for three cylinders for three-dimensional flow field analysis: (a) geometric model; (b) grid model, the space ratios being S/D = 1.35, 1.5, 1.7, 2, and aspect ratio being L/D = 10 (eliminating the influence of aspect ratio). In Figure 9b, the mesh scale near the cylinders is 0.005 m and the boundary layers are also adopted near the cylinder surfaces (the first layer height being 10^{-5} m, Y^+ = 0.22, and the number of grid cells being 650 thousand), and the dimensionless time step has the value 0.01 ($V\Delta t/D$ = 0.01).

Figure 11 shows the three-dimensional flow velocity contour, which verifies that in a three-dimensional flow field, the periodic flow regime of the wake region past three cylinders also occurs at S/D = 1.35 and 1.5, without the same phenomenon at S/D = 1.7 and 2.0, where the wake regime exhibits near-perfect symmetry. Therefore, the phenomenon of periodic flow regime of the wake region past three cylinders is intrinsic and related to Reynolds number and space ratio.

Evolution Process of the Periodic Flow Regime of the Wake Region

The asymmetrical gap flow between cylinders C1, C3 and C2, C3 reduces the periodic flow regime of the wake region past three cylinders directly at Re = 2 × 10^5, β = 60°, S/D = 1.5 or 1.35, and the coupling coherent influence of the wake past cylinder C1, C2 and the surface of cylinder C3 is the intrinsic cause.

Figure 12 shows the evolutionary process of the periodic flow regime of the wake region within a cycle. Figure 12a shows that the wake region past cylinder C3 deflects to cylinder C1, and the coherent vortex flow past three cylinders communicates with the wake region past cylinder C2; at time t+T/8, the wake region past cylinder C3 enlarges and the wake regions of cylinders C1 and C3 first communicate with each other. At the moment t+2T/8, the shedding vortex of the wake region past cylinder C1 propagates to the wake region downstream past three cylinders, the initial coherent vortex disappears, a

small-scale coherent vortex is formed, the wake of cylinder C3 is gradually biased towards cylinder C2, and there is no shedding vortex structure in the wake region of cylinder C2; at the moment t+3T/8, a coherent vortex is formed downstream of cylinder C3 to which the trailing zone of cylinder C1 is connected, the wake region of cylinder C3 is fully biased towards cylinder C2 and is separated from the downstream coherent vortex by the gap flow, and the trailing zone of cylinder C2 is also separated from the downstream coherent vortex. At the moment t+4T/8, the coherent vortex past three cylinders moves downstream, the trailing zone of cylinder C1 starts to separate from the coherent vortex, the initial fusion of trailing zones past cylinders C3 and C2 occurs, and the separation vortex forms at the end of the pile C2 trailing zone; at the moment of t+5T/8, the wake regions of cylinders C2 and C3 are fused, the shedding vortex of the flow field past cylinder C2 is gradually shed and propagates downstream, and the wake region of cylinder C3 starts to deflect; at the moment of t+6T/8, the shedding vortex behind cylinder C2 propagates downstream, a coherent vortex downstream is initially formed, and the wake region of cylinder C3 deflects to the cylinder C1; at the moment of t+7T/8, the coherent vortex scale behind three cylinders enlarges and develops gradually to maturity, the wake region of cylinder C2 is biased towards cylinder C1, the coherent vortex behind three cylinders separates from the wake of cylinder C1, and the wake of cylinder C2 is connected with the coherent vortex.

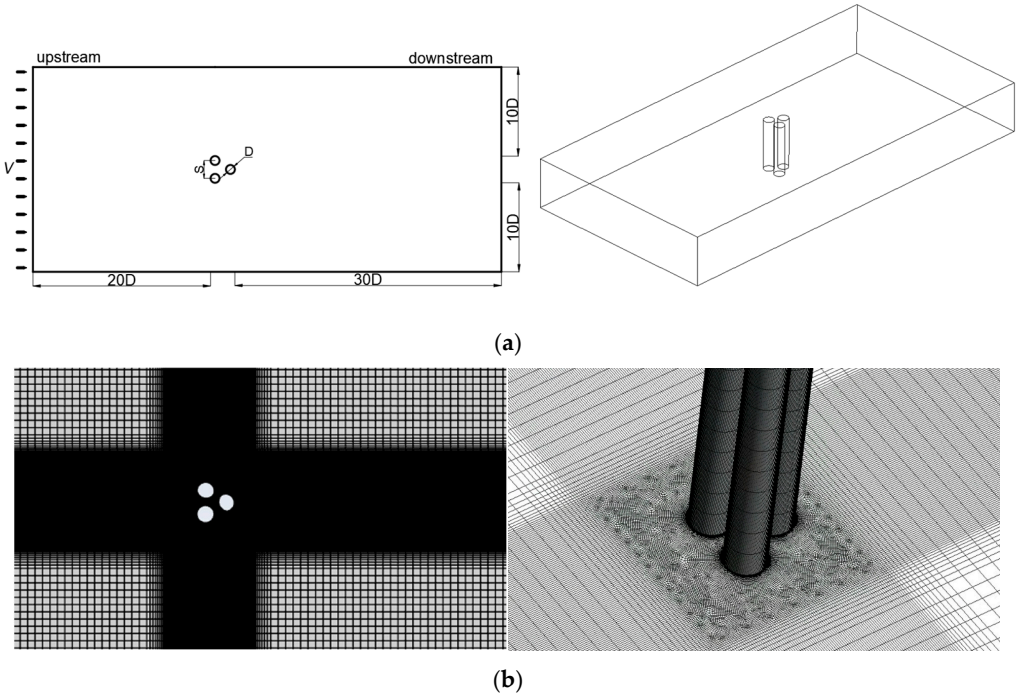
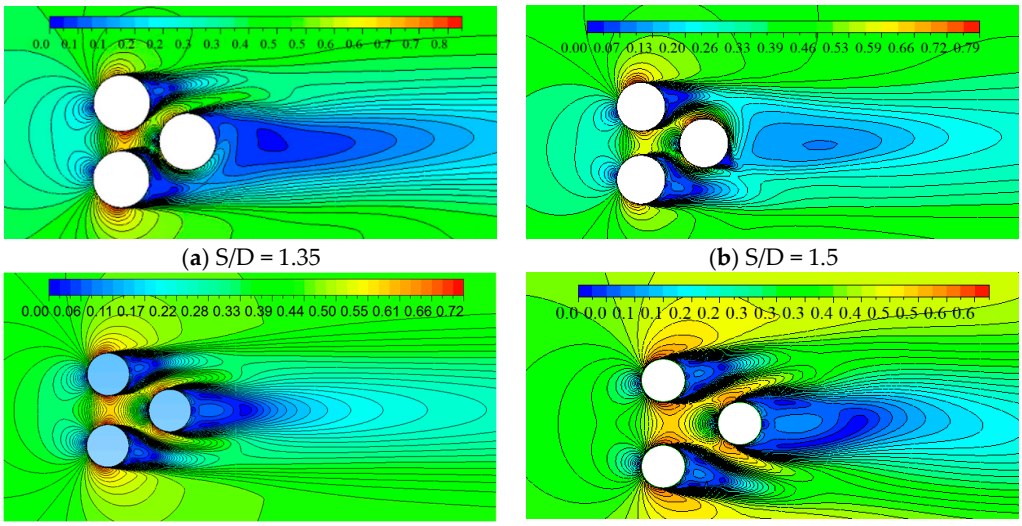


Figure 10. Arrangement for three cylinders: (**a**) geometric model; (**b**) grid model.

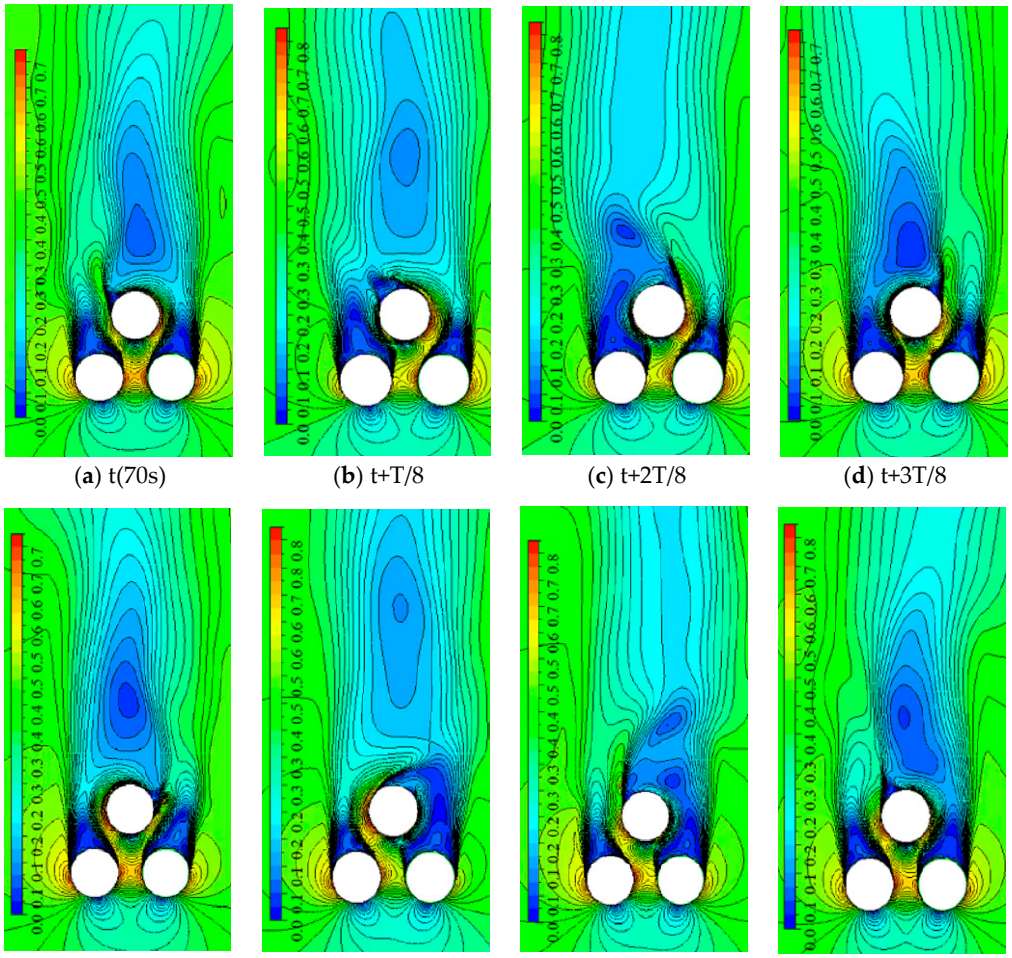
Consequently, from the viewpoint of the evolution law within the cycle of the wake region and the coherent vortex, the emergence of the periodic alternating flow is due to the periodic shedding of separation bubbles in the wake of cylinders C1 and C2, and the coherent vortex downstream of cylinder C3 evolves from the separation bubbles of the wake regions of cylinders C1 or C2. When separation bubbles exist in the wake region of cylinder C1, the coherent vortex evolves from the separation bubbles in the wake region behind cylinder C2 at the previous moment, and otherwise, it evolves from the separation bubbles behind cylinder C1 at the previous moment. Thus, for a certain gap ratio and Reynolds number conditions under the incidence angle of 60°, the emergence of a periodic flow regime in the wake region is the inevitable result because of the coherent effect of the flow field among cylinders C1, C2 and C3.



(**a**) S/D = 1.35 (**b**) S/D = 1.5

(**c**) S/D = 1.7 (**d**) S/D = 2

Figure 11. Three-dimensional flow velocity contours past three cylinders: (**a**) S/D = 1.35; (**b**) S/D = 1.5; (**c**) S/D = 1.7; (**d**) S/D = 2.0.



(**a**) t(70s) (**b**) t+T/8 (**c**) t+2T/8 (**d**) t+3T/8

(**e**) t+4T/8 (**f**) t+5T/8 (**g**) t+6T/8 (**h**) t+7T/8

Figure 12. Evolution of periodic flow regime during T.

3.2. Characteristics of Force Parameters

3.2.1. Pressure Coefficient Distributions around Cylinders

The pressure distribution around the cylinder surface under the influence of inter-cylinder gap flow for a three-cylinder scenario is significantly different from that in the case of flow past one cylinder. The gap flow increases the local velocity and reduces the local pressure, while the location of the stagnation point behind cylinders changes due to the presence of the gap flow.

Figures 13 and 14 show variation laws of surface pressure coefficient with spacing ratio S/D at incidence angle β = 0°and β = 60° in a subcritical regime. At incidence angle β = 0°, the surface pressure distribution of cylinder C1 exhibits symmetry, the pressure of the wake region of cylinder C1 rises and the Cp value increases due to the role of downstream cylinders C2 and C3, and with the increase of S/D, the Cp value of the wake region decreases gradually; the wake region of cylinder C1 is as the upstream of cylinders C2 and C3, and under the role of the inter-cylinder gap flow, the stagnation point of the surfaces of cylinders C2 and C3 deflects to the gap flow side, which for cylinder C2 is near 350° and for cylinder C3 is near 10°; when the value of S/D is smaller than four, the pressure coefficient around cylinders near the gap flow is slightly smaller and there is no controlling effect on pressure coefficient if the value of S/D is larger than four. At incidence angle β = 60°, gap flow occurs between cylinders C1 and C3 and also C2 and C3, and near the gap flow side, the pressure coefficient drops suddenly which leads to the stagnation point moving slightly to the side of the gap flow; the pressure coefficient distribution around cylinder C3 at the small spacing ratio of S/D = 1.5, 2, basically exhibits symmetry, and at S/D = 2.5, 3, because of the impact of the wake region behind cylinders C1 and C2, the pressure distribution exhibits asymmetry.

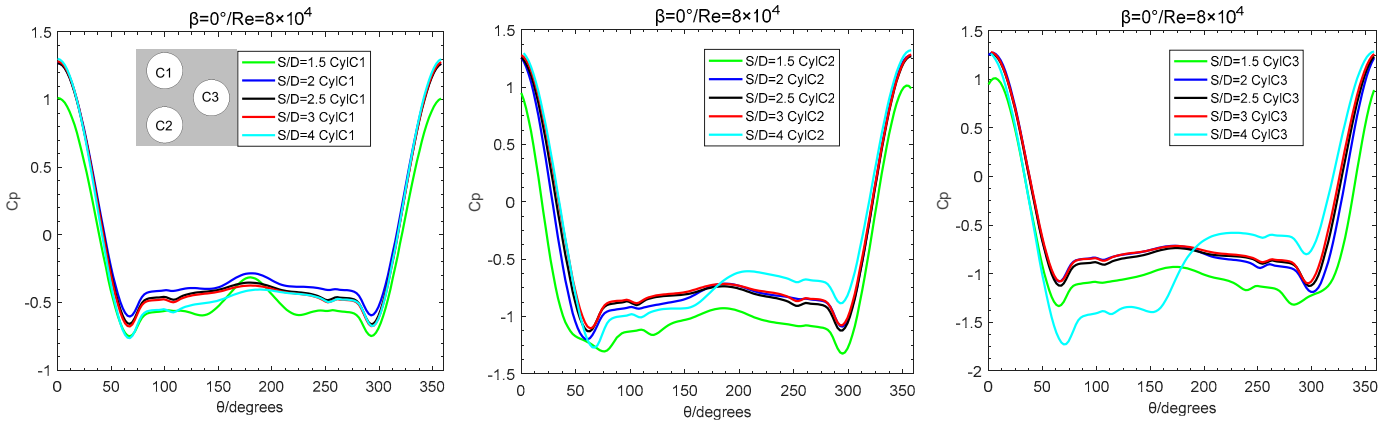
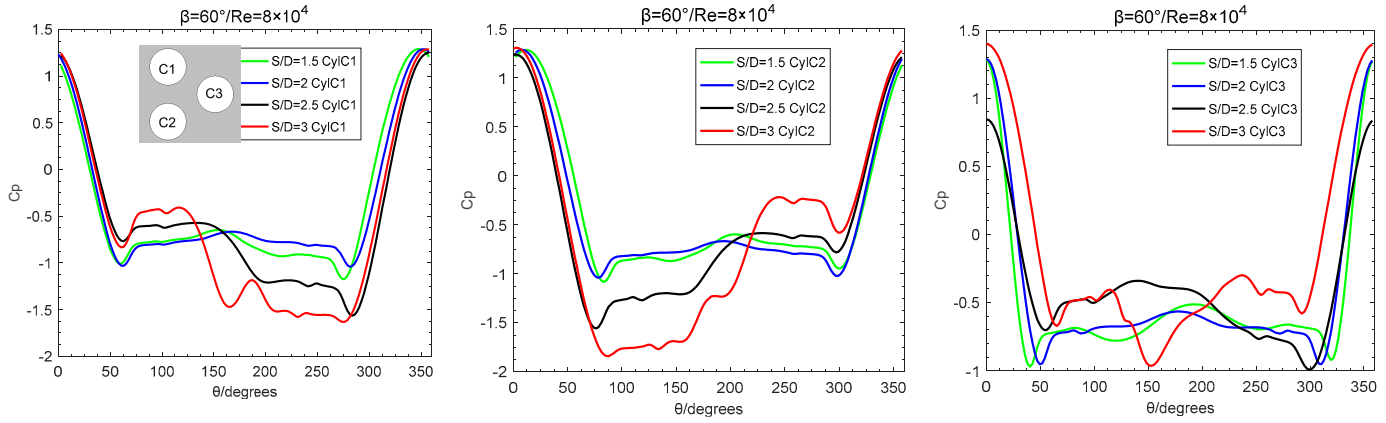


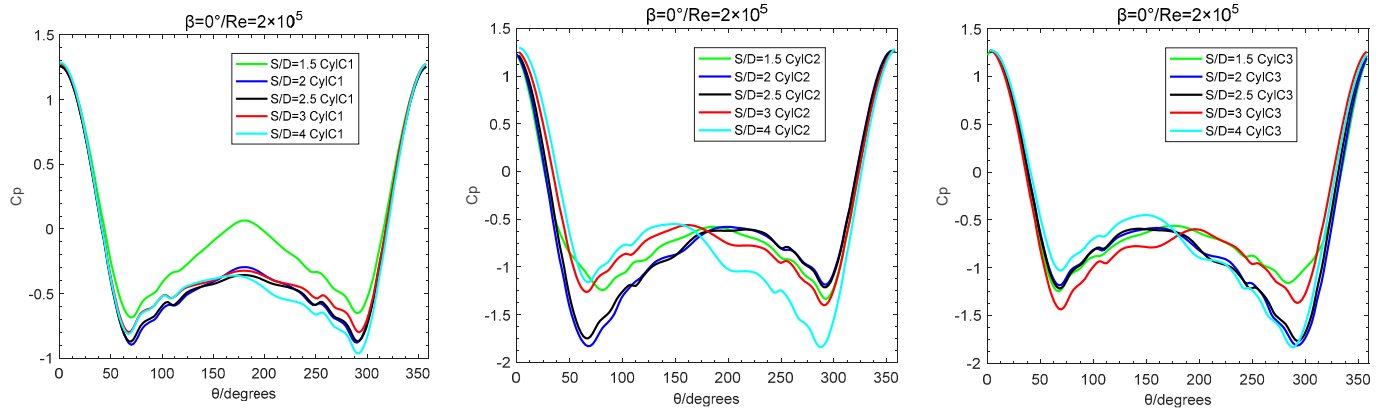
Figure 13. Variation of pressure coefficient of three cylinders with spacing ratio S/D: Re = 8 × 10^4, β = 0°; (**a**) C1; (**b**) C2; (**c**) C3.

In the critical regime, the characteristics of the cylinder surface pressure distribution are different from that in the subcritical regime. Figures 15 and 16 plot the changing rules of cylinder surface pressure coefficient with S/D in the critical regime. At incidence angle β = 0°, enlarging the spacing ratio S/D value from 1.5 to 4, the surface pressure coefficient of cylinder C1 is basically symmetrically distributed; for cylinders C2 and C3, the pressure coefficient around the cylinder near the gap flow is slightly smaller due to the role of the gap flow, and the stagnation point's location is on the opposite side. When the incidence angle β is 60°, the prominent phenomenon is that at S/D = 1.5, the periodic flow regime of the wake region or coherent vortex structure occurs, which is manifested by the surface pressure coefficient of cylinder C3 near the gap flow side steeply decreasing, and at the same time, the pressure coefficient of cylinder C2 near the gap flow side is small; when the opposite flow pattern occurs, cylinder C1 will show the same rule with cylinder C2.



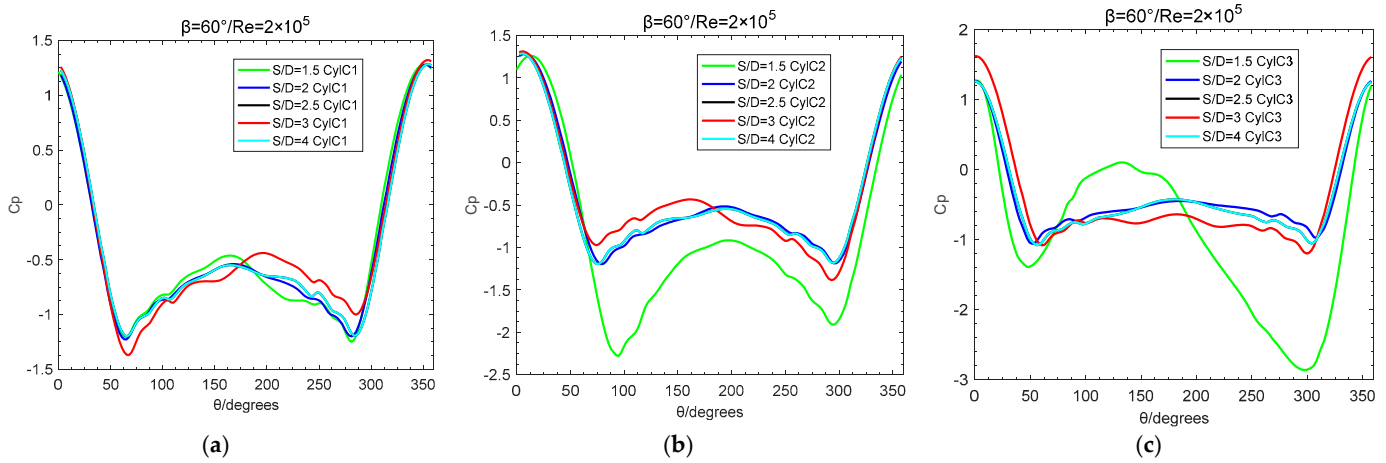
(**a**) (**b**) (**c**)

Figure 14. Variation of pressure coefficient of three cylinders with spacing ratio S/D:Re = 8 × 10^4, β = 60°; (**a**) C1; (**b**) C2; (**c**) C3.



(**a**) (**b**) (**c**)

Figure 15. Variation of pressure coefficient of three cylinders with spacing ratio S/D: Re = 2 × 10^5, β = 0°; (**a**) C1; (**b**) C2; (**c**) C3.



(**a**) (**b**) (**c**)

Figure 16. Variation of pressure coefficient of three cylinders with spacing ratio S/D: Re = 2 × 10^5, β = 60°; (**a**) C1; (**b**) C2; (**c**) C3.

Figures 17 and 18 plot the distribution of cylinder surface pressure coefficient with different S/D values in a supercritical regime. The cylinder surface pressure coefficient is

mainly affected by the wake region behind the cylinders, and the influence of the gap flow is not obvious compared to that in subcritical and critical regimes.

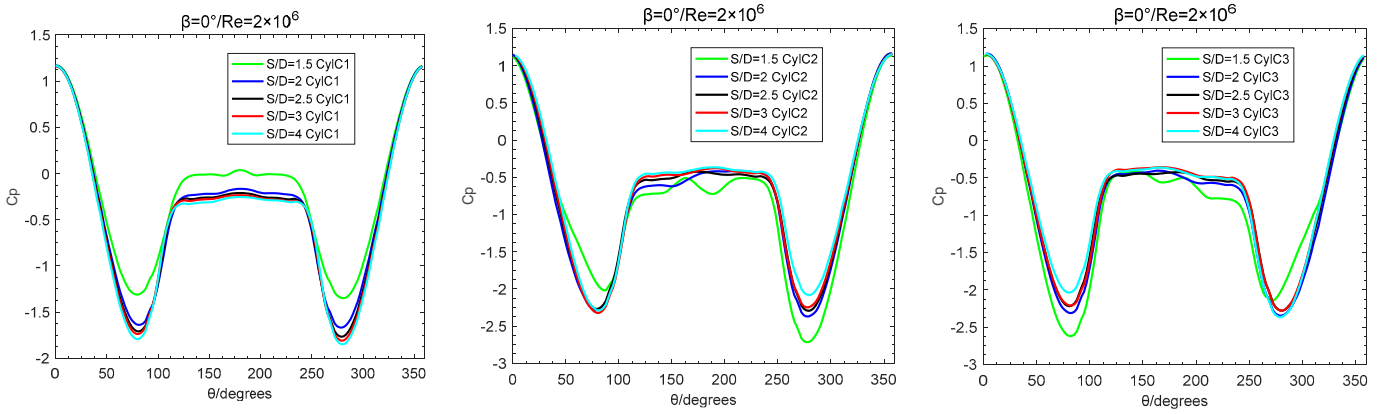


Figure 17. Variation of pressure coefficient of three cylinders with spacing ratio S/D:Re = 2 × 10^6, β = 0°; (**a**) C1; (**b**) C2; (**c**) C3.

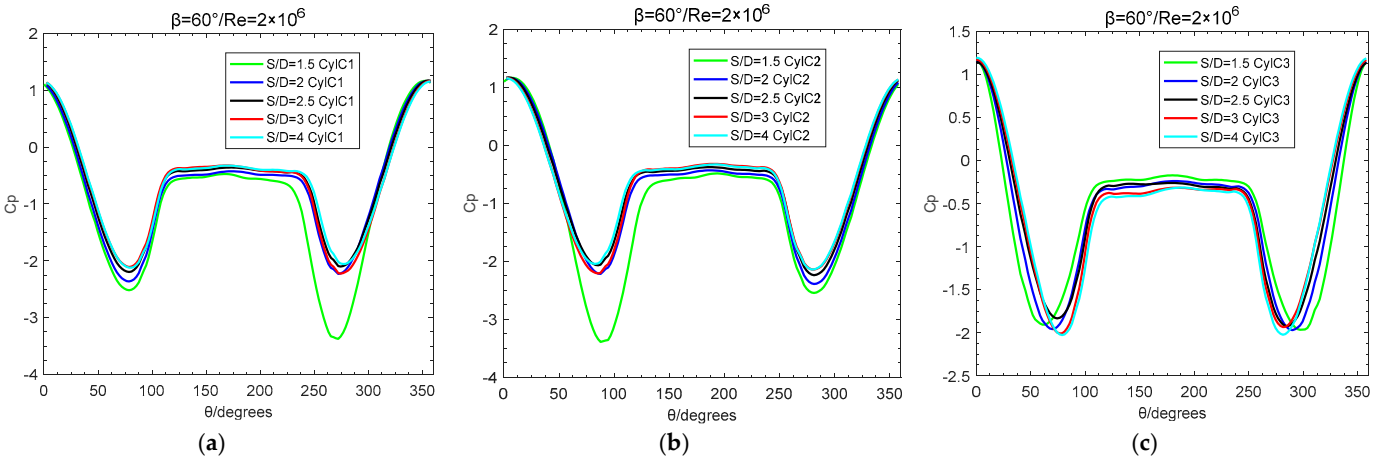


Figure 18. Variation of pressure coefficient of three cylinders with spacing ratio S/D:Re = 2 × 10^6, β = 60°; (**a**) C1; (**b**) C2; (**c**) C3.

3.2.2. Characteristics of Drag and Lift Coefficients

At β = 0°, Figure 19 shows the variation of the mean drag coefficients with S/D at different Reynolds numbers (8 × 10^4, 2 × 10^5, 2 × 10^6). For Re = 8 × 10^4, in Figure 19a, the mean drag coefficients for three cylinders C1, C2 and C3 increase with the enlargement of S/D from two to four; at S/D = 1.5, the mean drag coefficients (C1: 0.666, C2: 0.747, C3: 0.749) are far less than the value for a single cylinder (C_D = 1.18), which indicates that the upstream cylinder plays a significant role in reducing the mean value of the drag coefficients on the side-by-side downstream cylinders, and also that the downstream cylinders play a role in reducing the mean value of the drag coefficient of the upstream cylinder; with the enlargement of S/D, the interference among three cylinders attenuates, and the mean drag coefficient increases; at S/D = 4, the mean drag coefficients for three cylinders are 0.884 (C1), 1.061 (C2), and 1.128 (C3), respectively, indicating that the value of the cylinders C1 and C2 is close to the value (1.18) of a single cylinder, but the downstream cylinders play a role in reducing the mean value of the drag coefficient of the upstream cylinder, with the drag coefficient of C1 being 0.884. For Re = 2 × 10^5, the variation of mean drag coefficients for three cylinders C1, C2 and C3 with S/D exhibits a similar law with that for Re = 8 × 10^4: because of the interference among cylinders, the value of drag

coefficient is less than that of a single cylinder (approximately 1.08). For Re = 2 × 10^6, at 1.5 < S/D < 2.5, the drag coefficient for cylinder C1 increases with the enlargement of S/D, and at S/D > 2.5, the drag coefficient for cylinder C1 decreases with the enlargement of S/D; at 1.5 < S/D < 4, the drag coefficients for cylinders C2 and C3 are in a certain range 0.36~0.41 which is less than the value 0.73, which is the drag coefficient of a single smooth cylinder; in addition, at 1.5 < S/D < 4, the interference among cylinders still reduces the drag coefficient of three cylinders.

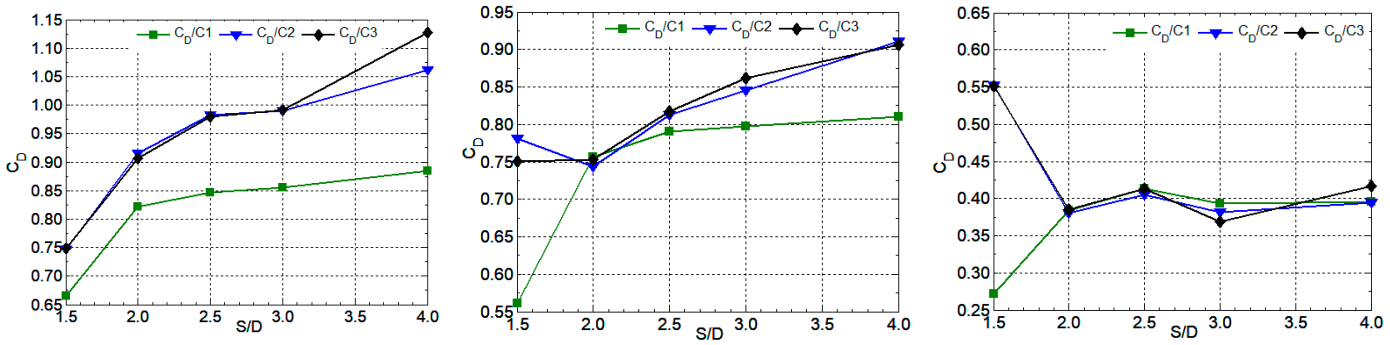
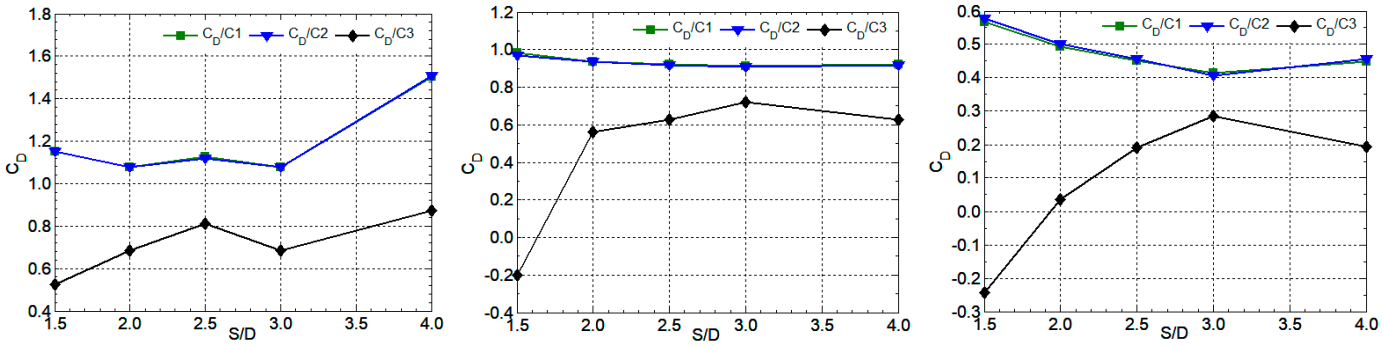


Figure 19. The variation of the mean drag coefficients with S/D (β = 0°): (**a**) Re = 8 × 10^4; (**b**) Re = 2 × 10^5; (**c**) Re = 2 × 10^6.

At β = 60°, Figure 20 shows the variation of the mean drag coefficients with S/D at different Reynolds numbers (8 × 10^4, 2 × 10^5, 2 × 10^6). For Re = 8 × 10^4, in Figure 20a, at 1.5 < S/D < 3, the drag coefficients of the side-by-side cylinders C1 and C2 decrease with the enlargement of S/D; at S/D = 1.5, drag coefficients are both 1.15. At S/D = 4, the drag coefficients for cylinders C1 and C2 are both 1.5, which is more than the value (1.18) for a single smooth cylinder; for cylinder C3, at 1.5 < S/D < 2.5, the drag coefficient increases with the enlargement of S/D, and at S/D = 3, the drag coefficient decreases, and increases if S/D > 3; the upstream side-by-side cylinders C1 and C2 play a significant role in reducing the mean value of the drag coefficients on downstream cylinder C3. For Re = 2 × 10^5, in Figure 20b, at 1.5 < S/D < 4, the drag coefficients of the side-by-side cylinders C1 and C2 decrease with the enlargement of S/D; at S/D = 1.5, the mean drag coefficients for cylinders C1 and C2 are 0.983 (C1), 0.969 (C2), respectively, and at S/D = 4, the values are both 0.919. For cylinder C3, at 1.5 < S/D < 3, the drag coefficient increases with the enlargement of S/D, and the drag coefficient increases if S/D >3; in addition, at 1.5 < S/D < 4, the interference among cylinders still reduces the drag coefficient of three cylinders, cylinder C3 being more prominent. For Re = 2 × 10^6, in Figure 19c, at 1.5 < S/D < 3, the drag coefficients of the side-by-side cylinders C1 and C2 decrease with the enlargement of S/D and slightly enlarge if S/D >3; at S/D = 1.5, the mean drag coefficients for cylinders C1 and C2 are 0.567 (C1), 0.576 (C2), respectively, and at S/D = 4, the values are 0.449 (C1), 0.456 (C2). For cylinder C3, at 1.5 < S/D < 3, the drag coefficient increases with the enlargement of S/D and the drag coefficient increases if S/D > 3; in addition, at 1.5 < S/D < 4, the interference among cylinders still reduces the drag coefficient of three cylinders.

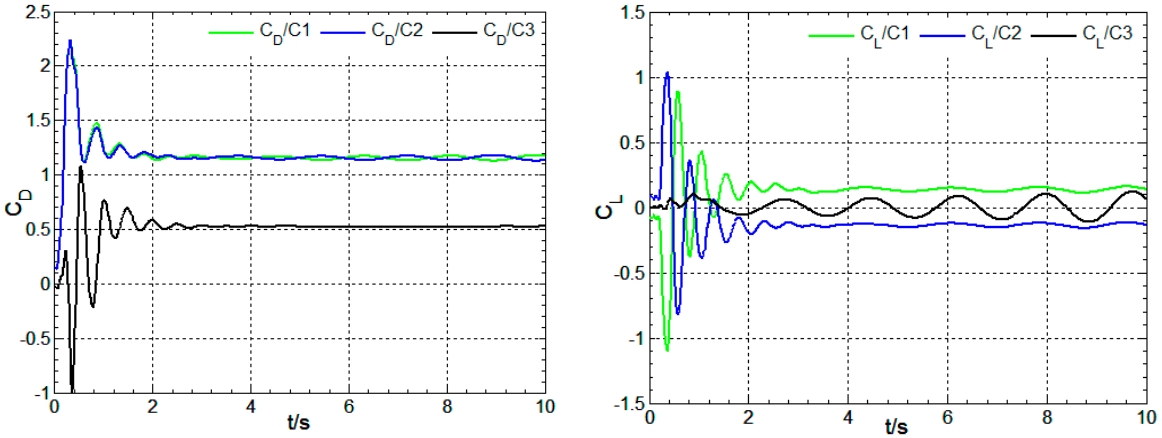
Figures 21–23 show the time-history variation of surface drag coefficient and lift coefficient (S/D = 1.5, β = 60°) with different Reynolds numbers (8 × 10^4, 2 × 10^5, 2 × 10^6). In Figures 21 and 23, the drag and lift coefficient curves with time show weaker fluctuating characteristics, which is compatible with the flow pattern in Figure 9. At S/D = 1.5, β = 60°, Re = 2 × 10^5, the periodic flow regime of the wake region past three cylinders is found, and the drag and lift coefficient curves with time are displayed in Figure 22. In Figure 22, the drag and lift coefficient curves with time exhibit strong fluctuating characteristics, the lift coefficient curve of cylinder C3 being more prominent. In Figure 22a, the drag coefficient curves of cylinders C1 and C2 exhibit anisotropic phases and have the same period; there is a certain phase difference between cylinder C3 and cylinders C1 and C2, and the phase

difference is unchanged with time. In Figure 22b, there are long-period and short-period signals in the lift coefficient curves over time of cylinders C1 and C2, the long period being mainly due to the coherent vortex structure in the wake region past three cylinders. For cylinder C3, the lift coefficient curve with time forms due to the effect of periodic flow regime in the wake region, displaying mainly a long-period signal, in which there is a strong fluctuating characteristic with a fluctuating amplitude close to 2.



(**a**) (**b**) (**c**)

Figure 20. The variation of the mean drag coefficients with S/D (β = 60°): (**a**) Re = 8 × 10^4; (**b**) Re = 2 × 10^5; (**c**) Re = 2 × 10^6.



(**a**) (**b**)

Figure 21. Time-history variation of surface drag coefficient and lift coefficient: Re = 8 × 10^4, S/D = 1.5, β = 60°; (**a**) drag coefficient; (**b**) lift coefficient.

Due to interference among cylinders, the time-history variation curves of surface drag and lift coefficients of three equally spaced cylinders compared with a single cylinder or larger S/D conditions exhibit significant changes in flow pattern and drag and lift characteristics. Especially, the effect of a periodic flow regime in the wake region among cylinders at S/D = 1.5, β = 60°, Re = 2 × 10^5 leads to changes in the frequency of mechanical properties around cylinders, and the main frequency is obviously reduced. If the mechanical data of a single cylinder is still used in the analysis of cylinder dynamic characteristics around three or more cylinders, it will introduce a lot of error in St or lift or drag.

3.3. Characteristics of Strouhal Number

Due to the interference of the wake regions among cylinders, the Strouhal number of the flow past three cylinders is no longer a single function of the Reynolds number and also changes with the incidence angle of the incoming flow and the pile spacing.

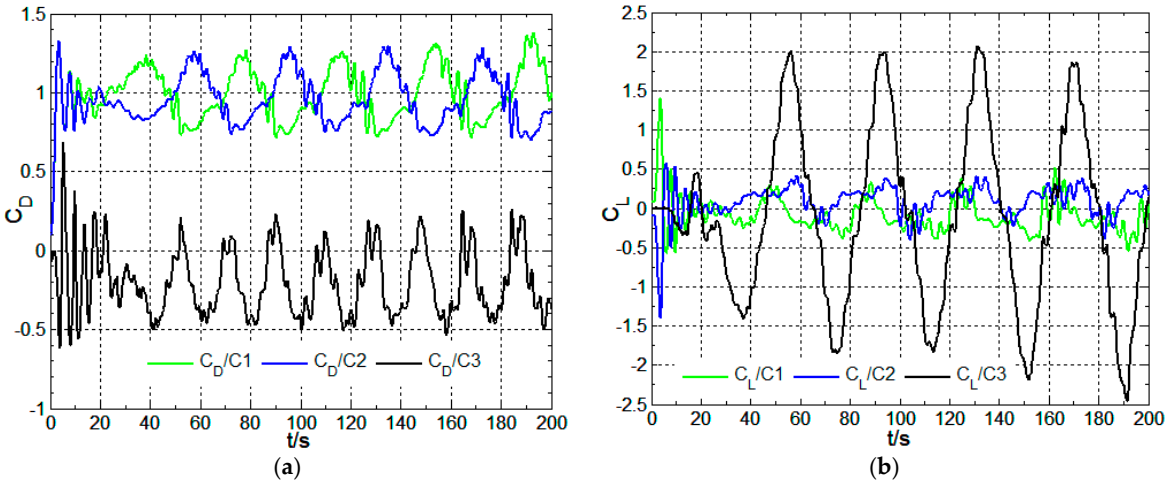


Figure 22. Time-history variation of surface drag coefficient and lift coefficient: Re = 2 × 10^5, S/D = 1.5, β = 60°; (**a**) drag coefficient; (**b**) lift coefficient.

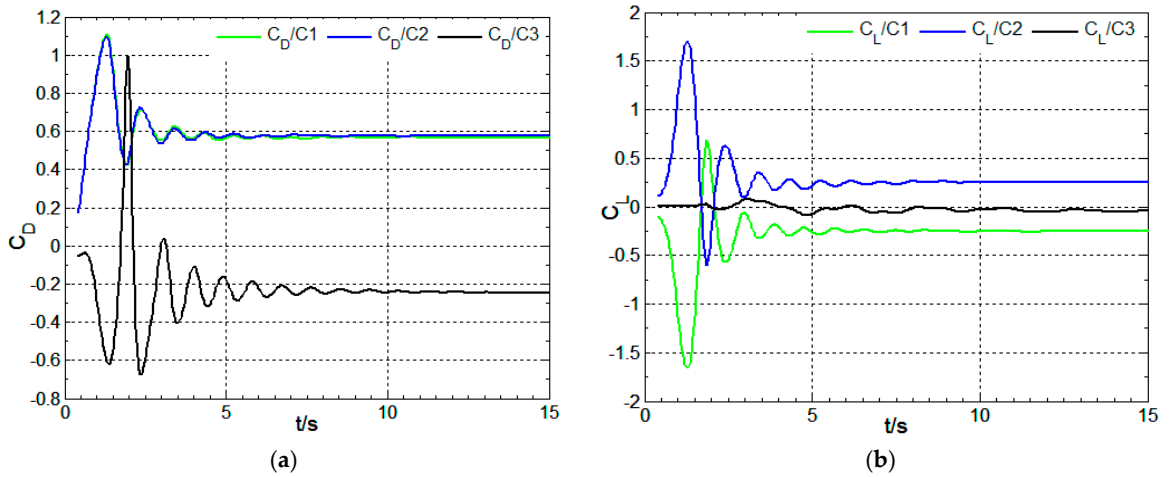


Figure 23. Time-history variation of surface drag coefficient and lift coefficient: Re = 2 × 10^6, S/D = 1.5, β = 60°; (**a**) drag coefficient; (**b**) lift coefficient.

Table 4 lists the Strouhal number of a single cylinder for different Reynolds numbers. Table 5 lists the Strouhal number for different spacing ratios, Reynolds numbers and incidence angles of flow past three equally spaced cylinders in the present work. At Re = 8 × 10^4, β = 0°, the St of cylinder C1 increases with the enlargement of the spacing ratio from 0.138 to 0.19, which is compatible with the results of Senlin Zheng et al. [13]; at S/D = 2.5, the Strouhal number of three cylinders is 0.19, which is close to the value 0.185. At Re = 2 × 10^5, β = 0°, the Strouhal numbers of three cylinders are 0.225 (C1) and 0.2 (C2, C3), which is more than that of a single cylinder. For Re = 2 × 10^6, β = 0°, the Strouhal number of cylinder C1 increases with the enlargement of spacing ratio from 0.167 to 0.213 and the Strouhal numbers of cylinders C2 and C3 are both 0.3 and 0.293 for S/D = 2.0, 2.5, respectively, which is less than the value for a single cylinder. At Re = 8 × 10^4, β = 60°, the Strouhal numbers of cylinders C1 and C2 decrease with the enlargement of spacing ratio from 0.263 to 0.212, which is far more than the value 0.185 of a single cylinder, but the Strouhal number of cylinder C3 increases with the enlargement of spacing ratio from 0.075 to 0.1, which is far less than the value 0.185 of a single cylinder, indicating that the interference of wake regions behind cylinders enlarges the Strouhal number of upstream cylinders C2 and C3 and reduces the Strouhal number of downstream cylinder C1. At Re = 2 × 10^5, 2 × 10^6, β = 60°, similar rules are displayed in Table 5; considering the effect of a periodic flow regime of the wake region among cylinders at S/D = 1.5, β = 60°

which is shown in Figure 21b, the period of lift coefficient curve for cylinder C3 is 37.73 s, corresponding to the Strouhal number 0.033 which is far less than the value 0.188 for a single cylinder; in addition, for cylinders C1 and C2, there are two types of cycles: a long cycle due to coherent vortex which is close to the value of cylinder C3, and a short cycle due to shedding vortex in the wake region corresponding to higher frequency and lower period.

Table 4. Strouhal number under different Reynolds numbers for a single cylinder.

Reynolds Number	**8×10^4**	**2×10^5**	**2×10^6**	**4×10^6**
Strouhal number	0.185 [4]	0.188 [4]	0.32	0.2 [16]

Table 5. Strouhal number for cylinders with different spacing ratios, Reynolds numbers and incidence angles.

Incidence Angle	**Spacing Ratio**	**Cylinder**	**Reynolds Number**		
			8×10^4	**2×10^5**	**2×10^6**
0°	1.5	C1	0.138		
		C2	0.181		
		C3	0.181		
	2	C1	0.150	0.225	0.167
		C2	0.175	0.200	0.300
		C3	0.175	0.200	0.300
	2.5	C1	0.190	0.225	0.213
		C2	0.190	0.200	0.293
		C3	0.190	0.200	0.293
60°	1.5	C1	0.263		
		C2	0.263		
		C3	0.075	0.033	
	2	C1	0.230	0.250	0.300
		C2	0.230	0.250	0.275
		C3	0.092	0.100	0.075
	2.5	C1	0.212	0.225	0.273
		C2	0.212	0.225	0.273
		C3	0.100	0.12	0.102

4. Conclusions

In this paper, a finite volume method with structured meshes based on the k-kl-ω turbulence model is used to simulate the flow around three cylinders in an equilateral triangular arrangement for two incidence angles, β = 0° and 60°, at Reynolds numbers 8×10^4, 2×10^5, and 2×10^6. Based on the present results, flow interference pattern characteristics among cylinders, characteristics of force parameters and characteristics of Strouhal number of each cylinder with different spacing ratios ranging from 1.5 to 4 at Re 8×10^4, 2×10^5 and 2×10^6 have been obtained. The main conclusions are drawn as follows:

(1) Based on the comparison of simulation results among different turbulence models, the model k-kl-ω simulates better results for flow around cylinders for the parameters of drag coefficient, root-mean-square value of the lift coefficient pulsation, Strouhal number St, basal pressure coefficient C_{pb}, and separation angle.

(2) The interference flow pattern past an equilateral triangle arrangement of cylinders is related to the Reynolds number, spacing ratio and incidence angle: (a) at Re = 3×10^4, 8×10^4, 2×10^5, β = 0°, the wake of the cylinders downstream (C2 and C3) exhibits symmetrical features, and a bi-stable flow regime did not appear in the present investigation. At Re = 5×10^5, 2×10^6, 4×10^6, a combined shedding vortex between two cylinders downstream appears in the wake of flow past three cylinders, and another obvious feature is that at Re = 5×10^5, 2×10^6, the vortex street is nearly symmetrically distributed in a transversal direction and asymmetrically distributed at Re = 4×10^6. (b) At Re = 3×10^4,

8×10^4, 5×10^5, 2×10^6, 4×10^6, $\beta = 60^\circ$, the flow fields exhibit near-perfect symmetry, when the cylinder (C3) downstream suppresses the wakes of the cylinders (C1 and C2) upstream; but at $Re = 2 \times 10^5$, the wake of the cylinder (C3) downstream displays asymmetrical features and a typical vortex appears downstream of cylinder C3.

(3) For the flow regime at $Re = 2 \times 10^5$, $\beta = 60^\circ$ and different spacing ratios, a periodic flow regime of the wake region past three cylinders is found for the first time. The periodic flow regime of the wake region past three cylinders also occurs at S/D = 1.35 and 1.5, without the same phenomenon at S/D = 1.7 and 2.0, where the wake regime exhibits near-perfect symmetry. Therefore, the phenomenon of periodic flow regime of the wake region past three cylinders is intrinsic, and related to Reynolds number and space ratio.

(4) Characteristics of force parameters of three cylinders are mainly affected by the interference among cylinders; at small spacing ratios such as S/D = 1.5, the pressure coefficient C_p and drag coefficient increase for the upstream cylinders and decrease for downstream cylinders; in addition, at $1.5 < S/D < 4$, the interference among cylinders reduces the drag coefficient of three cylinders with different Reynolds numbers.

(5) At $\beta = 60^\circ$, in subcritical and critical regimes, the Strouhal number of the upstream cylinders C1 and C2 is more than that of a single cylinder, and with the enlargement of the spacing ratio, the Strouhal number decreases; for the downstream cylinder C3, the Strouhal number is far less than that of a single cylinder and with the enlargement of the spacing ratio, the Strouhal number increases.

Author Contributions: Conceptualization, J.D.; methodology, J.D.; software, J.D.; validation, J.D.; formal analysis, J.D.; investigation, J.D.; resources, J.D.; data curation, J.D.; writing—original draft preparation, J.D. and G.Y.; writing—review and editing, J.D. and X.S.; visualization, J.D.; supervision, J.D.; project administration, G.Y.; funding acquisition, J.D. and G.Y. All authors have read and agreed to the published version of the manuscript.

Funding: This research was funded by Special Funds for Basic Research Operating Costs of Central-level Public Welfare Research Institutes (Y122006) and Jiangsu Funding Program for Excellent Postdoctoral Talent (2022ZB442).

Data Availability Statement: Data are contained within the article.

Acknowledgments: The authors acknowledge the funding support of Jiangsu Funding Program for Excellent Postdoctoral Talent.

Conflicts of Interest: The authors declare no conflicts of interest.

Nomenclature

List of symbols

Re	Reynolds number = $\rho VD/\mu$
S	distance between centers of two cylinders
D	the diameter of a cylinder
S/D	spacing ratio
β	incidence angle
St	Strouhal number $f \times D/V$
f	vortex shedding frequency
V	flow velocity
C_D	drag coefficient
C_L	lift coefficient
C_{pb}	basal pressure coefficient
C_p	pressure coefficient
Θ_s	separation angle
C'_L	lift coefficient pulsation

References

1. Wieselsberger, C. *New Data on the Laws of Fluid Resistance*; Technical report NACA-TN-84; NASA: Washington, DC, USA, 1921.
2. Roshko, A. Experiments on the flow past a circular cylinder at very high Reynolds number. *J. Fluid Mech.* **1960**, *10*, 345–356. [CrossRef]
3. Achenbach, E. Distribution of local pressure and skin friction around a circular cylinder in cross-flow up to Re = 5×10^6. *J. Fluid Mech.* **1968**, *34*, 625–639. [CrossRef]
4. Norberg, C. Fluctuating lift on a circular cylinder: Review and new measurements. *J. Fluids Struct.* **2003**, *17*, 57–96. [CrossRef]
5. Schewe, G. On the force fluctuations acting on a circular cylinder in cross flow from subcritical up to transcritical Reynolds numbers. *J. Fluid Mech.* **1983**, *133*, 265–285. [CrossRef]
6. Rodriguez, I.; Lehmkuhl, O.; Piomelli, U.; Chiva, J.; Borrell, R.; Oliva, A. LES-based study of the roughness effects on the wake of a circular cylinder from subcritical to transcritical Reynolds numbers. *Flow Turbul. Combust.* **2017**, *99*, 729–763. [CrossRef]
7. Ünal, U.O.; Atlar, M. An experimental investigation into the effect of vortex generators on the near-wake flow of a circular cylinder. *Exp. Fluids* **2010**, *48*, 1059–1079. [CrossRef]
8. Capone, A.; Klein, C.; Di Felice, F.; Miozzi, M. Phenomenology of a flow around a circular cylinder at sub-critical and critical Reynolds numbers. *Phys. Fluids* **2016**, *28*, 074101. [CrossRef]
9. Pereira, F.S.; Eça, L.; Vaz, G.; Girimaji, S.S. On the simulation of the flow around a circular cylinder at Re = 140000. *Int. J. Heat Fluid Flow* **2019**, *76*, 40–56. [CrossRef]
10. Sayers, A.T. Flow interference between three equispaced cylinders flow interference between three equispaced cylinders when subjected to a cross flow. *J. Wind Eng. Ind. Aerodyn.* **1987**, *26*, 1–19. [CrossRef]
11. Zdravkovich, M.M. The effects of interference between circular cylinders in cross flow. *J. Fluids Struct.* **1987**, *1*, 235–2261. [CrossRef]
12. Pouryoussefi, S.G.; Mirzaei, M.; Pouryoussefi, S.M.H. Force coefficients and Strouhal numbers of three circular cylinders subjected to a cross-flow. *Arch. Appl. Mech.* **2011**, *81*, 1725–1741. [CrossRef]
13. Zheng, S.; Zhang, W.; Lv, X. Numerical simulation of cross-flow around three equal diameter cylinders in an equilateral-triangular configuration at low Reynolds numbers. *Comput. Fluids* **2016**, *130*, 94–108. [CrossRef]
14. Bansal, M.; Yarusevych, S. Experimental study of flow through a cluster of three equally spaced Cylinders. *Exp. Therm. Fluid Sci.* **2017**, *80*, 203–217. [CrossRef]
15. Bao, Y.; Zhou, D.; Huang, C. Numerical simulation of flow over three circular cylinders in equilateral arrangements at low Reynolds number by a second order characteristic-based split finite element method. *Comput. Fluids* **2010**, *39*, 882–899. [CrossRef]
16. Lam, K.; Cheung, W.C. Phenomena of vortex shedding and low interference of three cylinders in different equilateral arrangements. *J. Fluid Mach* **1988**, *196*, 1–26. [CrossRef]
17. Tatsuno, M.; Amamoto, H.; Ishi-I, K. Effects of interference among three equidistantly arranged cylinders in a uniform flow. *Fluid Dyn. Res.* **1998**, *22*, 297–315. [CrossRef]
18. Meter, F.R. Two-equation eddy-viscosity turbulence models for engineering applications. *AIAA J.* **1994**, *32*, 1598–1605. [CrossRef]
19. DWalters, D.K.; Cokljat, D. A three-equation eddy-viscosity model for Reynolds-averaged Navier–Stokes simulations of transitional flow. *J. Fluids Eng.* **2008**, *130*, 121401. [CrossRef]
20. Mulvany, N.; Tu, J.Y.; Chen, L.; Anderson, B. Assessment of two-equation turbulence modelling for high Reynolds number hydrofoil flows. *Int. J. Numer. Methods Fluids* **2004**, *45*, 275–299. [CrossRef]
21. Meter, F.R. Performance of Popular Turbulence Models for Attached and Separated Adverse Pressure Gradient Flows. *AIAA J.* **2012**, *30*, 2066–2072. [CrossRef]

Disclaimer/Publisher's Note: The statements, opinions and data contained in all publications are solely those of the individual author(s) and contributor(s) and not of MDPI and/or the editor(s). MDPI and/or the editor(s) disclaim responsibility for any injury to people or property resulting from any ideas, methods, instructions or products referred to in the content.